Ethiopian Journal of Science and Sustainable Development

e-ISSN 2663-3205 *Volume 11 (1), 2024*

Journal Home Page: www.ejssd.astu.edu.et

Research Paper

Antibacterial and Antioxidant Compounds from Root Extracts of *Gloriosa superba* Linn: A Combined Experimental and Computational Study

Iman Mustefa[1], Milkyas Endale[2,*], Rajalakshmanan Eswaramoorthy[3]

[1]*Department of Applied Chemistry, Adama Science and Technology University, P.O.Box 1888, Adama, Ethiopia*
[2]*Traditional and Modern Medicine Research and Development Directorate, Armauer Hansen Research Institute (AHRI), P.O.Box 1242, Addis Ababa, Ethiopia*
[3]*Department of Biomaterials, Saveetha Dental College and Hospital, Saveetha University, Chennai 600 077, India*

Article Info

Article History:
Received 08 August 2023
Received in revised form 31 January2024
Accepted 09Febuary 2024

Keywords:
Antitumor, Antimicrobial, Anthelmintic, Anti-inflammatory, Antioxidant activity, Gloriosa superba, Molecular docking

Abstract

Throughout history, medicinal plants have globally served as remedies for various ailments, and diseases. The roots of *Gloriosa superba* are traditionally used to treat antitumor, antimicrobial, and anti-inflammatory diseases. In this study, the roots of *G. superba* (320 g) were successively extracted with *n*-hexane, chloroform, and methanol to afford 530 mg (0.17%), 2.89 g (0.90%), and 17.78 g (5.56%) yields, respectively. Silica gel column chromatographic separation of the combined chloroform and methanol extracts gave 4-methoxy caffeic acid heptyl ester (**1**), desmosterol (**2**), 3-hydroxymethyl phenol (**3**), 3-Hydroxy-5-methoxy-benzoic acid (**4**), sucrose (**5**) and rutinose (**6**). *In vitro* antibacterial study revealed promising zone of inhibition value by chloroform extract against *Klebsiella pneumoniae* (13±0.00 mm) compared to gentamicin (15.86±4.67 mm). Desmosterol (**2**), 3-hydroxymethyl phenol (**3**), and 3-Hydroxy-5-methoxy-benzoic acid (**4**) displayed promising zone of inhibition against *K. pneumonia* (12.33±0.58, 11.33±1.53 and 11.33±1.15 mm, respectively) at 1000 µg/mL compared to gentamycin (15.86±4.67 mm at 100 µg/mL). Promising inhibition zone values were also displayed by desmosterol (**2**) and 3-Hydroxy-5-methoxy-benzoic acid (**4**) against *Pseudomonas aeruginosa* (14±1.00 and 14±1.73 mm, respectively) compared to gentamycin (25±2.52 mm).Chloroform extract displayed 95.14% DPPH radical scavenging value compared to ascorbic acid (96.11%) at 200 µg/mL. Compounds **2** and **4** displayed binding affinities of -7.8 and -6.5 Kcal/mol, respectively, against PqsA protein of *P. aeruginosa*, compared to amoxicillin (-7.3 kcal/mol). Therefore, the *in vitro* antibacterial and radical scavenging activity results suggest the potential uses of the root extracts of *G. superba* as promising antibacterial agents and free radical scavengers.

1. Introduction

Medicinal plants have been employed as medicine by human civilizations from the dawn of time. These are still taken by a huge portion of the world's population, particularly in developing countries, like Ethiopia and have been proven to be beneficial in the treatment of various serious diseases, including cancer and various infections (Dar *et al*., 2017). *Gloriosa superba L.* (Figure 1), a member of the Colchicaceae/Liliaceae family of flowering plants, is known by the common names Yebab Mashila in Amharic and Harmel in Afan Oromo (Teklehaymanot, 2009; Belayneh and Bussa, 2014). It is an herbaceous medicinal climber that is widely distributed throughout Ethiopia and in the tropical and subtropical regions of Africa, including

*Corresponding author, e-mail: milkyasendale@yahoo.com

https://doi.org/10.20372/ejssdastu:v11.i1.2024.725

Senegal, Somalia, South Africa, and Zambia, as well as Southeast Asia, which includes India, Myanmar, Sri Lanka, and Malaysia. It is a stunning tuberous plant having vivid, red and yellow flowers with wavy edges that bloom especially during rainy seasons (Umavathi et al., 2020).

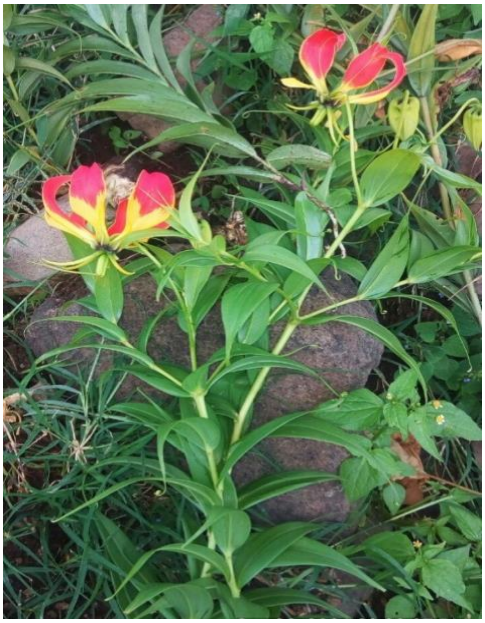

Figure 1: *Gloriosa superba* Linn (Photo taken by Iman Mustafa in Sep., 2021 from Doba, Western Hararge).

Preparation made from each component of *G. superba*, including tubers, leaves, seeds, and flowers, are used to cure ailments in Ayurveda and Yunani (Patil and Gavade 2012). It is rich in phytochemicals like alkaloids, glycosides, flavonoids, and saponins, which can act as antioxidants and may lower the risk of cancer and enhance heart health (Simon and Jayakumar, 2016). It is also used to treat cancer, gout, asthma, leprosy, arthritis, piles, ulcers, intestinal worms, bruising, infertility, skin problems, and impotence (Nikhila *et al*., 2016; Warrier *et al*., 1995). Moreover, it serves as an abortifacient, anthelmintic, and anti-inflammatory agent (Nikhila *et al*., 2016). However, it is a non-edible plant, and if ingested, it can be lethal, especially when administered in a high dose, the tuber is very toxic (Pallavi and Tulika, 2022; Tulika and Pallavi, 2020).

This plant is being used traditionally in Ethiopia to treat breast cancer. Its root part is chewed and applied externally to the affected breast (Ayele, 2018). Its crushed leaf filtrate is taken orally to treat Epilepsy (Belayneh and Bussa, 2014). Moreover, the plant is used to treat snakebite, impotence, stomachache, gout and tumor (Hassan and Roy, 2005; Solomon *et al*., 2020). Previous research has linked the medicinal uses of *G. superba* to the main secondary metabolites found in the seeds and tubers, such as tropolone-type alkaloids (Chaudhary *et al*., 2019; Jagtap and Rajendra, 2014).

In Ethiopia, there is currently no published research paper documenting the antibacterial, antioxidant activity, and phytochemical analysis of this plant. Despite the lack of scientific literature, local communities continue to rely on it for treating various ailments (Itefa and Tolessa, 2016). Thus, the aim of this study is to address this gap by presenting the isolation, spectroscopic identification, antibacterial and antioxidant evaluation, along with *in silico* molecular docking and drug likeness properties of compounds isolated from *G. superba roots.*

2. Materials and Methods

2.1. Plant material collection and identification

The plant material was collected from Doba district of Western Hararge Zone, Ethiopia. The area is located at about 378 km to the east of Addis Ababa. The identification of the plant material was done with the help of Botanist Melaku Wendaferash at the Department of Biology, National Herbarium of Ethiopia, Addis Ababa University (voucher code: IM001).

2.2. Preparation of plant material and extraction

The collected rhizome of *G. superba* was cut into smaller pieces and dried under shade. Then it was pulverized into a fine powder using a mechanical grinder. The powder was stored in air tight containers at room temperature till further experimentation.

The root powder of *G. superba* (320 g) was soaked into 2 L *n*-hexane for 72 h and shaken with mechanical shaker at room temperature. The solution was filtrated, and concentrated using a rotary evaporator at around 40 ^{o}C to afford *n*-hexane crude extract. The marc left was soaked in 2 L chloroform for 72 h. The mixture was filtered, and dried to afford chloroform crude extract. Finally, the marc left was further extracted in 2 L methanol for 72 h followed by filtration and dried to afford methanol crude extract. The extracts' thin layer chromatography (TLC) profiles were checked to identify appropriate eluent for column separation.

2.3. Isolation of compounds

The crude extracts of chloroform and methanol were combined as they showed similar TLC profiles. The combined crude extract (15 g) was adsorbed onto 15 g of silica gel (mesh size 60-120), and subjected to silica gel column chromatography (165 g of silica gel) using *n*-hexane for initial packing. Elution was carried out with increasing gradient of ethyl acetate in *n*-hexane followed by increasing gradient of methanol in dichloromethane. A total of 171 fractions (50 mL each) were collected. Fractions that showed identical retention factor (R_f) values and the same characteristic color on TLC were combined.

Fraction 10 (eluted with 20% EtOAc in *n*-hexane) was washed with *n*-hexane and afforded compound **1** (14.4 mg) as white powder. Fraction 13 (eluted with 30% EtOAc in *n*-hexane) afforded compound **2** (14.2 mg) as pale-yellow powder. Fraction 16 and 17 (eluted with 30% EtOAc in *n*-hexane) combined to afforded compound **3** (17.4 mg) as a pale-yellow needle-like compound. Fractions 35-40 (eluted with 40% EtOAc in *n*-hexane) were combined and washed with *n*-hexane to afford compound **4** (12.8 mg) as pale-yellow needles. Fractions 165 and 168 (eluted with 100% methanol) afforded compound **5** (100.8 mg) as white powder and compound **6** (169.3 mg) as reddish-brown powder after washing the crude extracts with DCM.

2.4. Structure elucidation

Nuclear magnetic resonance (NMR) spectroscopic techniques were employed to elucidate the structure of isolated compounds. The ^{1}H NMR, ^{13}C NMR, and DEPT-135 were obtained using Bruker Avance 400 MHz spectrometer at the Department of Chemistry, Addis Ababa University. Solvents, DMSO (d_6) and $CDCl_3$, were utilized for the analysis.

2.5. Antibacterial activity

In vitro antibacterial activities of the crude extracts and isolated compounds of *G. superba* root were studied against six pathogenic bacterial strains; namely, *E. faecalis* (ATCC 29212), *S. aureus* (ATCC 25923), *E. coli* (ATCC 25922), *K. pneumoniae* (ATCC 700603), *P. aeruginosa* (ATCC 27853), and *S. typhimurium* (ATCC 13311) retrieved from Adama Public Health Research and Referral Lab Center. Mueller-Hinton agar plates were inoculated with the standardized inoculum of the test micro-organisms (corresponding to 0.5 McFarland turbidity standard). Six sterile filter paper disks (Whatman No. 1 of ~6 mm in diameter) were impregnated with 20 µL of desired concentrations of either the crude, isolated compounds or controls (gentamicin as positive control and dimethyl sulphoxide (DMSO) as negative control), and placed on the inoculated agar surface. These plates were incubated under suitable conditions, at 37 °C for 24 h (CLSI 2018, Jonasson *et al*., 2020). The diameters of the growth inhibition zones around each disc were then measured in mm using a sliding caliper.

2.6. Antioxidant activity

Antioxidant activities of the extracts and isolated compounds were measured based on their free radical scavenging activity, which was determined by the 1,1-diphenyl-2-picryl-hydrazyl (DPPH) method. 0.04 % DPPH solution was prepared by dissolving 0.004 g DPPH in 100 mL methanol. The solution was kept in darkness for 30 min to complete the reaction. The crude extracts and isolated compounds were serially diluted as 1000, 500, 250, 125 µg/mL crude extracts and 100, 50, 25, 12.5 µg/mL isolated compounds. To each 1 mL of serially diluted solutions, 4 mL of 0.04% DPPH was added to get 200, 100, 50, 25 µg/mL crude extracts and 20, 10, 5, 2.5 µg/mL isolated compounds. The resulting solutions were placed in the dark for 30 min and then subjected to a UV-Vis spectrophotometer to record absorbance at 517 nm. Ascorbic acid with a similar concentration of test samples was used as the positive control. The DPPH radical scavenging activity of each of the tested compounds was reported by percentage inhibition using the following formula (Brand-Williams *et al*., 1995).

$$\textit{Radical scavenging activity (\%)} = \frac{Ab_{standard} - Ab_{analyte}}{Ab_{standard}} * 100$$

2.7. *In silico* molecular docking of the isolated compounds

A molecular docking study was carried out to evaluate the manner of binding of the most effective drugs against target proteins by docking isolated compounds (**2** and **4**) into the active site of proteins

using AutoDock Vina and a standard protocol (Seeliger and de Groot, 2010; Trott and Olson 2010). The chemical structures of compounds **2** and **4** were drawn with the ChemOffice tool (Chem Draw 16.0) and assigned with the proper 2D orientation, and the energy of each molecule was minimized with ChemBio3D. The energy-minimized ligand molecules were then fed into AutoDock Vina to perform the docking simulation. The protein data bank was used to download the crystal structures of the receptor molecules DNA gyrase B of *E. coli* (PDB ID: 6F86), PqsA of *P. aeruginosa* (PDB ID:5OE3) and pyruvate kinase of *S. aureus* (PDB ID:3T07).

Using the reported standard protocol, the protein was prepared by removing the co-crystallized ligand, selected water molecules and cofactors. The target protein file was prepared by leaving the associated residue with protein using Auto Preparation of target protein file Auto Dock 4.2. (MGL tools 1.5.7). The grid box for docking simulations was set using the graphical user interface program. The grid was designed to surround the region of interest in the macromolecule. To find the best-docked conformation between ligand and protein, the docking algorithm provided with AutoDock Vina was used. For each ligand, a maximum of nine conformers were considered during the docking process. Conformations with the most favorable (least) free binding energy were selected for analyzing the interactions between the target receptor and ligands by Discovery studio visualizer and PyMOL.

2.8. *In silico* drug-likeness and toxicity predictions

The isolated compounds were evaluated for their pharmacokinetic profiles by *in silico* methods for predicting their molecular properties using Lipinski's Rule of Five (Lipinski 2016) and the Veber rule (Veber *et al*., 2002). The physicochemical and pharmaco-kinetics properties of the compounds were estimated using ADME descriptors by SwissADME (http://www.swissadme.ch/), online server. To estimate *in silico* and pharmaco-kinetic parameters and other molecular properties, the isolated compound structures were submitted to SwissADME tools and converted to their canonical simplified molecular-input line-entry system "SMILEs". The organ toxicity profiles and toxicological endpoints of the isolated compounds and toxicity classes were predicted using the Pro Tox II web server explore (https://toxnew.charite.de/).

2.9. Statistical analysis

The experimental results were expressed as mean ± standard deviation (SD) of three replicates. Microsoft Excel 2016 statistical package was used for all analyses.

3. Results and Discussion

3.1. Extraction yield

The plant materials (roots) of *G. superba* were successively extracted with *n*-hexane, chloroform, and methanol to afford 530 mg (0.17 %), 2.89 g (0.90%), and 17.78 g (5.56 %) yields, respectively.

3.2. Characterization of isolated compounds

Compound **1** was isolated with R_f value of 0.3 (10% EtOAc in *n*-hexane as visualizing agent). Its ^{1}H-NMR spectrum (400 MHz, $CDCl_3$) (Table 1) revealed the existence of two aromatic protons with AB spin pattern at δ 6.94 (d, J = 8.0 Hz, 1H) and 7.09 (d, J = 8.1 Hz, 1H). Two oxygenated protons were observed at δ 3.95 (s, 3H) and 4.21 (t, J = 6.7 Hz, 2H) attributed to methoxy and oxygenated methylene, respectively. The presence of an olefinic proton signal at δ 6.31 (d, J = 15.9 Hz, 1H) and 7.63 (d, J = 15.9 Hz, 1H) were observed. Methylene and terminal methyl protons were observed at δ 1.71 (m, 2H), 1.61 (s, 2H), and δ 0.90 (t, J = 6.4 Hz, 3H), respectively.

The ^{13}C-NMR spectrum (100 MHz, $CDCl_3$) (Table 1) in combination with DEPT-135 displayed 17 carbon signals corresponding of which the peaks at δ_C 55.9 and δ_C 64.6 belong to methoxy and oxygenated methylene carbons, respectively, whereas the peak δ_C 14.1 suggests a terminal methyl group. Six methylene carbon signals were observed at δ_C 64.6, 31.9, 29.4, 28.8, 26.0, and 22.7 of which the first one is linked to heteroatom oxygen. The presence of two olefinic methine carbons was observed at δ_C 114.7 and 144.6. Ester carbonyl carbon appeared at δ_C 167.4 whereas six aromatic carbons at δ_C 147.9, 146.7, 127.1, 123.0, 117.6, and 115.7, of which peaks at δ_C 127.1, 147.9, and 146.7 disappeared in DEPT-135, suggesting these peaks belong to quaternary carbons.

Table 1: ^{1}H NMR and ^{13}C NMR data ($CDCl_3$) of 4-methoxy caffeic acid heptyl ester (**1**)

Carbon Position	^{1}H-NMR	^{13}C-NMR	^{1}H-NMR data of caffeoyl moiety (Takenaka *et al.*, 2003)	^{13}C-NMR data of caffeoyl moiety (Takenaka *et al.*, 2003)
1	-	127.1	-	127.8
2	7.09 (d, *J* = 8.1 Hz, 1H)	115.7	7.024 (d, J= 2.0 Hz)	115.3
3	-	146.7	-	146.8
4	-	147.9	-	149.8
5	6.81 (d, J= 12.9 Hz)	117.6	6.758 (d, J = 8.3 Hz)	116.5
6	6.94 (d, *J* = 8.0 Hz, 1H)	123.0	6.920 (d, J = 8.3 Hz)	123.3
7	7.63 (d, J = 15.9 Hz, 1H)	144.6	7.529 (d, J = 15.8 Hz)	147.9
8	6.31 (d, J = 15.9 Hz, 1H)	114.7	6.231 (d, J = 15.8 Hz)	114.4
9	-	167.4	-	167.8
1’	0.90 (t, *J* = 6.4 Hz, 3H)	14.1		
2’	1.71 (m, 2H)	22.7		
3’		31.9		
4’		28.8		
5’		26.0		
6’	1.61 (s, 2H)	29.4		
7’	4.21 (t, J = 6.7 Hz, 2H)	64.6		
1’’	3.95 (s, 3H)	55.9		

The presence of the deshielded sp^2 methine (δ_C 144.6) suggests the presence of alpha beta conjugated system. Methylene signals pointed down in DEPT-135 spectra, in good agreement with the ^{13}C NMR spectral data. The spectral data suggest that compound **1** is 4-methoxy caffeic acid heptyl ester (**1**, Figure 2), isolated herein for the first time from the species.

Compound **2** was isolated with R_f value of 0.4 (20% EtOAc in *n*-hexane as visualizing agent). The ^{1}H NMR (400 MHz, $CDCl_3$) (Table 2) spectrum displayed signals of olefinic methine protons at δ 5.4 (brs, 1H) and 5.1 (brs, 1H), sp^3 oxygenated methine proton signal at δ 3.7 (m, H-3), and methylene proton adjacent to the oxygenated methine at δ 2.4. Five methyl signals of which four of them appeared as singlets at δ 0.7, 1.0, 1.6, and 1.9 confirming the methyl groups are attached to quaternary carbons, and one multiplate at δ 0.9.

The ^{13}C NMR (100 MHz, $CDCl_3$) (Table 2) spectrum displayed the presence of five methyl carbons which resonated at δ_C11.9, 14.1, 19.4, 19.8, and 22.7. Ten methylene carbon signals were observed resonating at δ_C 21.1, 24.3, 26.1, 28.3, 31.6, 33.7, 36.2, 36.5, 37.3 and 39.8. The presence of five methine carbons were observed at δ_C 31.9, 33.9, 50.1, 51.2, and 56.8. The peaks observed at δ 42.3 and 45.8 in the ^{13}C NMR spectrum were sp^3 quaternary carbon atoms that belong to C-10 and C-13, respectively. The spectrum also showed sp^3 oxygenated methine at δ 71.8 (C-3) and olefinic carbons at δ 121.7 (C-6 and C-24), 132.2 (C-25), and 140.7 (C-5) of which the latter belong to quaternary carbon. The above spectral data are in good agreement with data reported in the literature for desmosterol (Wilson *et al*., 1996, Figure 2), reported herein for the first time from the species. Desmosterol (**2**) is the immediate precursor of cholesterol in the Bloch pathway of cholesterol biosynthesis. 24-dehydrocholesterol reductase catalyzes the reduction of desmosterol to cholesterol.

Table 2: ^{1}H NMR and ^{13}C NMR data ($CDCl_3$) of desmosterol (**2**)

Position	^{1}H-NMR	^{13}C-NMR	^{1}H-NMR (Wilson *et al*., 1996)	^{13}C-NMR data (Wilson *et al*., 1996)
1		36.5	1.078 ,1.845	37.2
2		31.6	1.838, 1.500	31.6
3	3.7 (s, 1H)	71.8	3.500	71.8
4		42.3	2.294, 2.235	42.3
5	-	140.7	-	140.7
6	5.4 (s, 1H)	121.7	5.400	121.7
7		33.7	1.529, 1.973	31.9
8		31.9	1.454	31.8
9	0.9 (m, 6H)	50.1	0.929	50.1
10	-	37.3	-	36.5
11		21.1	1.50, 1.46	21.1
12		39.8	1.158, 2.011	39.7
13	-	45.8	-	42.3
14	0.9 (m, 6H)	56.8	0.989	56.7
15		28.3	1.577, 1.072	24.3
16		26.1	1.839, 1.266	28.2
17		51.2	1.102	56.0
18	0.7 (s, 3H)	11.9	0.680	11.8
19	1.0 (s, 3H)	19.4	1.009	19.4
20		33.9	1.396	35.6
21	0.9 (m, 6H)	19.8	0.937	18.6
22		36.2	1.408, 1.041	36.1
23	2.02 (s, 2H)	24.3	1.849, 2.021	27.7
24	5.1 (s, 1H)	121.7	5.100	125.2
25	-	132.2	-	130.9
26	1.9 (s, 3H)	22.7	1.682	25.7
27	1.6 (s, 3H)	14.1	1.602	17.6

Compound **3** was isolated with R_f value of 0.25 (20% EtOAc in *n*-hexane as eluent). Its ^{1}H-NMR spectrum (400 MHz, DMSO-d_6) (Table 3) revealed the existence of ABX spin system aromatic protons at δ 7.0 (m, 2H), 7.3 (d, J = 7.4 Hz, 2H), and 6.8 (m, 2H). The presence of oxygenated methylene proton was displayed at δ 4.48 (d, J = 4.8 Hz, 2H). The ^{13}C NMR spectrum (100 MHz, DMSO-d_6) (Table 3) in combination with DEPT-135 showed oxygenated methylene carbon signal at δ_C 58.7 and six aromatic carbon signals at δ_C 115.0, 119.1, 127.8, 128.9, 144.3 and 154.6 of which the later suggest the presence of oxygenated sp^2 quaternary carbon. The above spectral data suggest that the compound is 3-hydroxymethyl phenol (**3**, Figure 2), reported herein for the first time from the plant. Previously of 3-hydroxymethyl phenol (**3**) was isolated from *Aspergillus nidulans*, and was demonstrated to possess significant biotechnological and pharmacological potential since it exhibited broad spectrum antimicrobial and anti-biofilm activities (Kumar *et al.*, 2017).

Compound **4** was isolated with R_f value of 0.25 (30% EtOAc in *n*-hexane as visualizing agent). Its ^{1}H-NMR spectrum (400 MHz, DMSO-d_6) (Table 4) revealed the existence of three aromatic protons at δ 7.20 (d, J = 8.2 Hz, 1H) and 6.49 (d, J = 14.3 Hz, 2H) suggesting a trisubstituted aromatic ring. The presence of methoxy group was observed at δ 3.7 (s, 3H).

The ^{13}C NMR spectrum (100 MHz, DMSO-d_6) (Table 4) in combination with DEPT-135 displayed eight carbon signals of which the presence of carboxyl carbonyl, and two sp^2 oxygenated quaternary carbons were observed at δ_C 169.0, δ_C 157.3, and 158.1,

respectively. Methoxy carbon was also evident at δ_C 56.2. Three sp2 methines were evident at δ 102.6, 109.2, and 110.8 whereas sp^2 quaternary carbon appeared at δ 131.9. The disappearance of peaks at δ 169.0, δ 157.3, 158.1 and δ 131.9 complement these carbons are quaternary carbons. The spectral data suggest that the compound is 3-Hydroxy-5-methoxy-benzoic acid (**4**, Figure 2), reported herein for the first time from the plant.

Compound **5** was isolated as with R_f value of 0.65 (20% MeOH in DCM as visualizing agent). Its ^{1}H-NMR spectrum (400 MHz, DMSO-d_6) revealed anomeric proton at δ 5.2 (d, J = 3.8 Hz, 1H). Oxygenated methylene was observed at δ 4.9 (s, 2H). The ^{13}C NMR spectrum (100 MHz, DMSO-d_6) in combination with DEPT-135 displayed twelve carbon signals corresponding to three methylene carbon signals resonating at δ_C 60.9 and 62.5, and anomeric carbon signals resonating at δ_C 104.5 and 92.2. Carbon bearing a hydroxy functional group were also apparent from δ_C 70.3 to 82.9. DEPT-135 spectra displayed peaks at δ_C 62.6 and 60.9 pointing down in good agreement with the presence of two oxygenated methylene carbons. The above spectral evidence supports the compound is a disaccharide sugar composed of glucose and fructose subunits. Thus, based on the spectral data the compound was identified as sucrose (**5**, Figure 2). Previously, sucrose crystals were grown using the isolated fraction from the methanol extract of the rhizome powder of *G. superba* (Gopinath *et al*., 2015).

Table 3: ^{1}H NMR and ^{13}C NMR data (DMSO-d_6) of 3-hydroxymethyl phenol (**3**)

Position	^{1}H-NMR	^{13}C-NMR	^{1}H-NMR (Kumar *et al.*, 2017)	^{13}C-NMR (Kumar *et al.*, 2017)
1	-	144.3	-	142.66
2	7.0 (m, 1H)	119.1	6.86 (br, s)	119.07
3	-	154.6	-	155.95
4	6.8 (m, 1H)	127.8	6.89 (1H, dd, J = 7.3 and 1.5)	144.62
5	7.3 (d, *J* = 7.4 Hz, 1H)	128.9	7.22 (1H, dd, J = 7.3 and 7.2)	129.83
6	6.8 (m, 1H)	115.0	6.75 (1H, dd, J = 7.2 and 1.5)	113.77
1’	4.48 (d, *J* = 4.8 Hz, 2H)	58.7	4.65 (2H, s)	65.07 (CH_2-OH)

Table 4: ^{1}H NMR and ^{13}C NMR data (DMSO-d_6) of 3-Hydroxy-5-methoxy-benzoic acid (**4**)

Position	^{1}H-NMR	^{13}C-NMR	^{1}HNMR (Legrand *et al*., 2004)	^{13}C-NMR (Legrand *et al*., 2004)
1'		169.0		165.95
1	-	131.9	-	131.35
2	6.49 (d, *J* = 14.3 Hz, 1H)	110.8	6.91 (s, 1 H	105.99
3	-	158.1	-	160.35
4	7.20 (d, *J* = 8.2 Hz, 1H)	102.8	6.97 (s, 1 H	104.99
5	-	157.3	-	158.53
6	6.49 (d, *J* = 14.3 Hz, 1H)	109.2	6.58 (s, 1 H	108.54
2'	3.7 (s, 3H)	56.2	3.82 (s, 3 H)	55.15

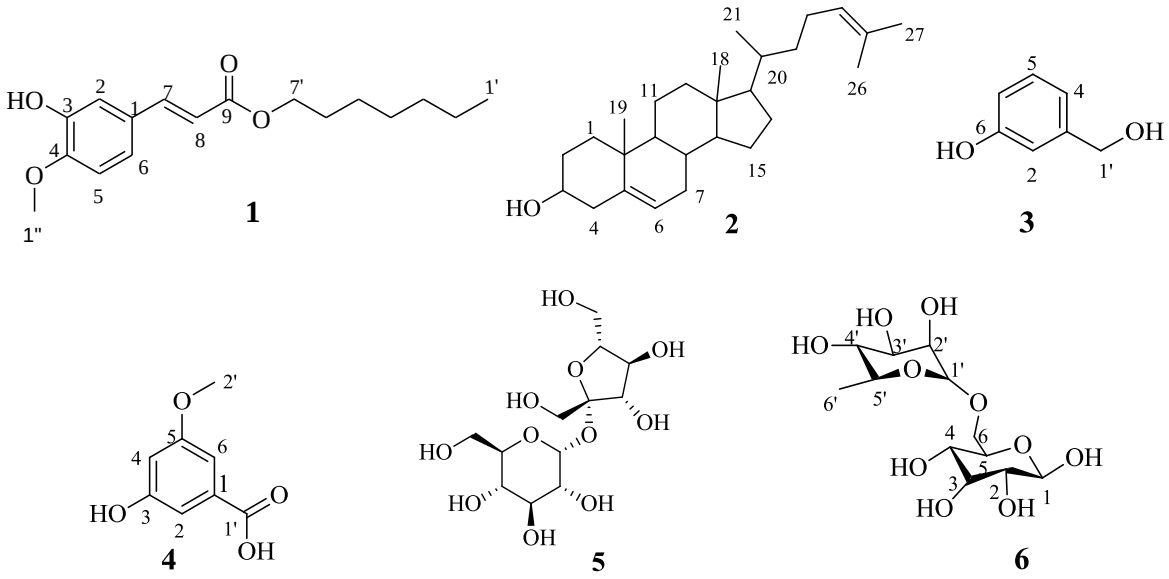

Figure 2: Structure of compounds isolated from roots of *G. superba* Linn

Compound **6** was isolated with R_f value of 0.62 (20% MeOH in DCM as eluent). Its ^{1}H-NMR spectrum (400 MHz, DMSO-d_6) exhibited two doublets 5.2 (d, J = 3.7 Hz, 1H) and 3.9 (d, *J* = 8.2 Hz, 1H) that are assigned for the anomeric protons of the glucose, H-1 and rhamnose H-1' moieties, respectively. The latter signal along with the multiplate observed at δ 1.3 (m, 3H) for a secondary methyl group was evident for the presence of rhamnopyranose moiety. The spectrum also exhibited a series of peaks in the region between 4.00-3.00 accounting for the presence of oxygenated methine protons. The ^{13}C NMR spectrum (100 MHz, DMSO-d_6) in combination with DEPT-135 displayed twelve carbon signals of which two anomeric carbons at δ 104.3 (C-1') and 92.2 (C-1) and one oxymethylene at δ_C 60.8. Oxygenated methines carbons were evident in between δ 77.5 to 62.5. Moreover, a methyl signal was observed δ 17.9. The obtained spectral evidence supports a disaccharide sugar containing a rhamnose and glucose subunits. Thus, based on the spectral data, the compound was identified as 6-O-α-L-rhamnosyl-D-glucose (rutinose (**6**), Figure 2).

3.3. Antibacterial activity

The antibacterial activity of crude extracts and isolated compounds was evaluated by measuring the size of the zone of inhibition against the test organisms (Table 5 and 6). The extracts displayed promising growth inhibitory effect at the concentration of 200 mg/mL against the selected bacterial strains. The *n*-hexane extract showed highest zone of inhibition (13.33±0.58 mm) against *E. coli*, followed by inhibition against *S. typhimurium* and *K. pneumoniae* with the zone of inhibition values of 12.67±0.58 and 11.0±1.00 mm, respectively. The finding is promising in comparison to the standard drug (gentamicin). The drug showed inhibition zones of 26.71±2.36, 28.86±2.34, and 21.67±2.55 mm against *E. coli*, *S. typhimurium* and *K. pneumoniae*, respectively. Similarly, the chloroform extract exhibited growth inhibition effect against *K. pneumoniae, S. typhimurium, S. aureus,* and *E. coli* with mean inhibition zones of 13.00±0.00, 13.00±1.00, 12.33±0.58 and 12.00±1.00 mm, respectively.

The MeOH extract was also found to be the only one active against *P. aeruginosa* (11.33±0.58 mm) and *E. faecalis* (12.00±0.0 mm) at higher concentration but inactive in lower concentrations. The extract also displayed activity against *E. coli* (11.67±1.15 mm) and *K. pneumoniae* (10.00±1.00 mm). In comparison to the *n*-hexane and MeOH extract, (at smaller concentration of 25 mg/mL) the chloroform extract showed the highest mean inhibition zone of (11.00±0.00 mm) against *K. pneumoniae* and (10.67±0.58 mm) against *S. typhimurium* and *E. coli* (Table 5).The efficacy of antimicrobial activity depends on the nature and volume of active principles present in the tested extracts. The extracts showed better inhibitory activity of methanol against *P. aeruginosa* and *E. faecalis* among the tested

bacteria might be attributed to active secondary metabolites, including alkaloids, which are efficiently controlled by these organisms compared to others (Babu *et al.*, 2018).

According to Megala and Elango (2012), *G. superba* tuber and seed extracts showed appreciable antibacterial effect against the tested *E. coli, K. pneumoniae, P. mirabilis, P. aeruginosa,* and *S. aureus*. The results showed that the dichloromethane extract exhibited pronounced inhibition against all the tested organisms. The maximum inhibition was observed on *P. mirabilis* in dichloromethane tuber extract 16 mm and *E. coli* in methanol tuber extract 15 mm and *S. aureus* in methanol tuber extract 15 mm. *K. pneumoniae* was found to be moderately suppressed by methanol tuber extract 14 mm and acetone seed extract 14 mm, followed by *P. aeruginosa* methanol seed extract 14 mm compared to the positive control, streptomycin (Megala and Elango, 2012).

These activities can be due to the potential ability of the secondary metabolites to shape a complex with extracellular proteins and with the cell wall of microorganisms. The higher inhibition effect of the extracts might be due to better solubility of those secondary metabolites, which showed the presence of a wide spectrum of antibiotic compounds (Jothi, *et al*., 2019). As a result, phytochemical compounds mainly phenolic ones and alkaloids may be responsible for *G. superba's* antibacterial activity.

Similar experiments on the isolated compounds showed antibacterial activity *in vitro* with mean inhibition zones displayed in the range between 6.67 and 15.00 mm for tested bacterial strains (Table 6). Among the isolated compounds, the *in vitro* antibacterial activity displayed by compound **3** showed highest activity both at higher and lower concentrations (15.00±0.00 and 11.00±0.00 mm at 1 mg/mL and 125 µg/mL respectively) against *S. typhimurium* compared to gentamicin (28.86±2.34mm at 100 µg/mL). Compounds **2** and **4** showed relatively strong antibacterial activity (14.00±1.00 mm and 14.00±1.73 mm at 1 mg/mL) against *P. aeruginosa* compared to gentamicin (25.00±2.52 mm at 100 µg/mL) while the others did not show activity (Table 6). Compounds **2-4** displayed comparable activity (11.33±1.53, 10.00±1.73 and 11.67±1.15mm, respectively at 500 µg/mL) against *K. pneumoniae* compared to gentamicin (15.86±4.67mm at 100 µg/mL) while compound **4** showed higher activity (13±1.00mm at 1 mg/mL) against *E. coli*, and the only one active against *E. faecalis* (12.33±0.58 mm at 100 µg/mL) (Table 6).

Table 5: Antibacterial activity of *G. superba* root extracts against selected bacterial strains

Extract	Conc. (mg/mL)	Inhibition Diameter (mm)±SD					
		E. coli	*P. aeruginosa*	*K. pneumoniae*	*E. faecalis*	*S. typhimurium*	*S. aureus*
***n*-Hexane**	200	13.33±0.58	NE	11±1.0	NE	12.67±0.58	NE
	100	13.33±0.58	NE	10.33±1.15	NE	10.67±0.58	NE
	50	12±1.00	NE	9.33±1.15	NE	9.67±0.58	NE
	25	10.67±1.53	NE	9±1.73	NE	9.33±1.15	NE
Chloroform	200	12±1.00	NE	13±0.00	NE	13±1.00	12.33±0.58
	100	12±1.00	NE	12.33±0.58	NE	12±1.00	NE
	50	10.67±0.58	NE	11.67±0.58	NE	11.67±0.58	NE
	25	8.33±1.53	NE	11±0.00	NE	10.67±0.58	NE
Methanol	200	11.67±1.15	11.33±0.58	10±1.00	12±0.00	NE	NE
	100	11±1.00	10±1.00	10±1.00	NE	NE	NE
	50	11±1.00	NE	11.33±0.58	NE	NE	NE
	25	8.33±2.08	NE	8±0.00	NE	NE	NE
Gentamycin	100	26.71±2.36	25±2.52	15.86±4.67	NE	28.86±2.34	25.43±2.15

NE – No effect

Table 6: The antibacterial activities of isolated compounds **1-4** against selected bacterial strains

Compound	Conc (µg/mL)	Inhibition Diameter (mm)±SD					
		E. coli	*P. aeruginosa*	*K. pneumoniae*	*E. faecalis*	*S. typhimurium*	*S. aureus*
1	500	11.33±0.58	NE	NE	NE	10.33±0.58	NE
	250	10±1.00	NE	NE	NE	9.33±0.58	NE
	125	10±0.00	NE	NE	NE	8.33±0.58	NE
	62.5	8.33±0.58	NE	NE	NE	7.33±0.58	NE
2	1000	10.67±1.15	14±1.00	12.33±0.58	NE	15±0.00	12.67±1.15
	500	10±1.73	13.67±0.58	11.67±1.15	NE	14±2.00	12.33±1.15
	250	8.33±2.52	12±1.00	11.33±1.53	NE	11.33±0.58	12±.00
	125	7.67±2.89	10.67±0.58	10.33±0.58	NE	11±0.00	9.33±2.08
3	500	NE	NE	11.33±1.53	NE	8.33±0.58	NE
	250	NE	NE	10±1.00	NE	7.33±1.15	NE
	125	NE	NE	9±1.00	NE	NE	NE
	62.5	NE	NE	7.33±0.58	NE	NE	NE
4	1000	13±1.00	14±1.73	11.33±1.15	12.33±0.58	11.33±0.58	10.67±0.58
	500	11.67±0.58	12.33±1.53	10±1.73	11.33±0.58	10±0.00	9.67±0.58
	250	10.66±1.15	10.67±0.58	9.67±1.53	8.67±2.31	8.67±0.58	7±0.00
	125	NE	10±1.00	7±1.00	7±1.00	8±0.00	NE
Gentamycin	100	26.71±2.36	25±2.52	15.86±4.67	NE	28.86±2.34	25.43±2.15

NE – No effect

3.4. Antioxidant activity

In the DPPH scavenging assay of crude extracts of *G. superba*, reduction of DPPH radical was accompanied by a decrease in absorbance at 517 nm. The DPPH radical was greatly reduced by the crude extracts, especially by the chloroform extract. At a concentration of 200 µg/mL, the DPPH radical scavenging activities (%) were found to be 27.11, 72.98, and 95.14 for *n*-hexane, methanol, and chloroform extracts, respectively (Table 7).

The DPPH radical scavenging activity (%) of aqueous, ethanolic, and benzene extracts of *G. superba* tubers were reported to be 65.575±0.183, 91.786±0.050, and 55.939±0.154, respectively, at a concentration of 200 µg/mL (Jayakumar *et al*., 2018). In another study, different concentrations of methanolic extracts at 100 µg of *G. superba* whole plant parts, namely shoot, flower, tuber, showed a radical scavenging activity 65.76, 60.34, 80.12 µg/mL, respectively.

The DPPH scavenging activities were found to decrease as the concentration of the samples in the assay got reduced. The positive control (ascorbic acid) showed a maximum scavenging effect at very low and high concentrations (88.63 - 96.11%). Compared to the standard ascorbic acid, the DPPH radical scavenging activities of the extracts were found to be lower except for the chloroform extract that showed comparable activity with lower IC_{50} value (5 µg/mL) which corresponds to its strong antioxidant activity.

The DPPH radical scavenging activities of isolated compounds were found to be 33.57, 35.69, 28.86 and 23.14 for compounds **1, 2, 3** and **4,** respectively (Table 8). For the various concentrations, compounds **1** and **2** exhibited higher percent inhibition as compared to **3** and **4**. When related to the standard ascorbic acid, the DPPH radical scavenging activities of isolated compounds were generally found to be lower (Table 8).

3.5. *In silico* molecular docking

The molecular docking study was carried out to assess the binding affinities and binding interactions of isolated compounds **2** and **4** with target proteins *E. coli* DNA gyrase B (PDB ID: 6F86), *S. aureus* Pyruvate Kinase (PDB ID: 3T07), *P. aeruginosa* PqsA (PDB ID: 5OE3), and Human Peroxiredoxin 5 (PDB ID: 1HD2).

Table 7: DPPH radical scavenging activities (%) of *G. superba* root extract

Conc (µg/mL)	Control	Extracts						Positive control	
		Hexane		Chloroform		Methanol		Ascorbic Acid	
		A	%RSA	A	%RSA	A	%RSA	A	%RSA
200	1.029	0.75	27.11	0.05	95.14	0.278	72.98	0.04	96.11
100	1.029	0.831	19.24	0.134	86.98	0.543	47.23	0.045	93.68
50	1.029	0.852	17.20	0.247	75.996	0.67	34.89	0.047	90.57
25	1.029	0.854	17.01	0.314	69.48	0.8	22.25	0.05	88.63
IC_{50}		424.3		5.7		110		0.0007	

A-Absorbance, RSA-Radical Scavenging Activity, IC_{50} – 50% Inhibitory Concentration

Table 8: DPPH radical scavenging activities (%) of isolated compounds **1-4**

Conc. (µg/mL)	Control	Compounds								Positive Control	
		1		**2**		**3**		**4**		Ascorbic Acid	
		A	%RSA	A	%RSA	A	%RSA	A	%RSA	A	%RSA
20	1.275	0.847	33.57	0.820	35.69	0.907	28.86	0.980	23.14	0.028	97.80
10	1.275	0.910	28.63	0.872	31.61	0.972	23.76	1.019	20.08	0.045	96.47
5	1.275	0.954	25.18	0.875	31.37	0.985	22.75	1.033	18.98	0.573	55.06
2.5	1.275	0.973	23.69	0.890	30.20	1.076	15.61	1.094	14.20	0.875	31.37
IC_{50}		50		40		140		600		4	

A-Absorbance, RSA-Radical Scavenging Activity, IC_{50} – 50% Inhibitory Concentration

The binding affinity, amino acid residues that are involved in hydrogen bonds, hydrophobic, and van der Waals interactions at each ligand- protein complexes were mapped using AutoDock Vina (Tables 9-11). The docked compounds **2** and **4** displayed minimum binding energies - 6.7 and -5.7 kcal/mol, -4.7 and -3.4 kcal/mol, -7.8 and -6.5 kcal/mol, and -4.6 and -4.9 kcal/mol with DNA gyrase B, Pyruvate Kinase, and PqsA, respectively (Tables 9-11). Such low docking score values signify good interactions of the compounds with protein binding pocket.

In the study, these isolated compounds (**2** and **4**) demonstrated comparable to better binding affinity (binding energy of - 6.7 and - 5.7 kcal/mol) against protein DNA gyrase than the standard drug, amoxicillin (−6.1 kcal/mol). Both compounds have showed hydrogen bonding interactions. Compound **2** showed H-bonding interaction with amino acid residues Asn-46 and compound **4** showed interaction with Gly-77, Asp-73, and Thr-165 as showed in Table 9 below. Also, both compounds exhibited more residual Van der Waals interaction than the standard drug amoxicillin (3D and 2D binding interactions of compounds **2**, **4** and amoxicillin against DNA gyrase B (PDB ID: 6F86) are included in SI appendix 18).

The binding affinities of the ligands (**2** and **4**) to the protein Pyruvate Kinase (-3.4 and -4.7 kcal/mol) were found to be equal to or less than amoxicillin (-4.7 kcal/mol). Of these, the strongest binding affinity was displayed by compound **2** (-4.7 kcal/mol). Both compounds showed H-bonding interaction. Compound **2** showed H-bonding interaction with amino acid Thr-353 and Thr-348, and compound **4** showed interaction with Ala-358 (Table 10). 3D and 2D binding interactions of compounds **2**, **4** and amoxicillin against Pyruvate Kinase (PDB ID: 3T07) are included in SI appendix 19).

When docked to the protein PqsA, compound **2** displayed higher binding affinity (-7.8 kcal/mol) as compared to the standard drug, amoxicillin (-7.3 kcal/mol), where compound **4** showed the binding affinity (-6.5 kcal/mol) that is lower than the standard drug. In the interaction with PqsA, compound **4** displayed H-bonding interactions with amino acid Ala-303 (Table 11). 3D and 2D binding interactions of compounds **2**, **4** and amoxicillin against PqsA (PDB ID: 5OE3) are included in SI appendix 20).

Table 9: Molecular docking value of isolated compounds (**2** and **4**) against DNA gyrase B (PDB ID: 6F86)

Compounds	Affinity (kcal/mol)	H-bond	Residual interactions	
			Hydrophobic	Van der Waals interaction
2	-6.7	Asn-46	Arg-76, Ile-78, Pro-79	Ala-47, Asp-73, Thr-165, Glu-50, Gly-77, Arg-136
4	-5.7	Gly-77, Thr-165, Asp-73	Glu-50, Ile-78	Ile-94, Pro-79, Arg-76, Gly-75, Ala-47
Amoxicillin	-6.1	Asp-73, Arg-76, Asn-76, Gly-77	Pro-79	Ile-94, Thr-165, Arg-136

Table 10: Molecular docking value of isolated compounds (**2** and **4**) against Pyruvate Kinase (PDB ID: 3T07)

Compounds	Affinity (kcal/mol)	H-bond	Residual interactions	
			Hydrophobic	Van der Waals interaction
2	-4.7	Thr-353, Thr-348	Ala-358, Ile-361	Lys-349, Ser-362, Ser-354
4	-3.4	Ala-358	Ile-361	Ile-359, Thr-353, Ser-354
Amoxicillin	-4.7	Thr-464, Thr-463, Leu-355, Ala-358	Ala-358, Ile-359	Ser-361, Ser-362

Table 11: Molecular docking value of isolated compounds (**2** and **4**) against PqsA (PDB ID: 5OE3)

Compounds	Affinity (kcal/mol)	H-bond	Residual interactions	
			Hydrophobic	Van der Waals interaction
2	-7.8	-	Ser-280, Pro-281, His-394, Ile-301, Phe-209, Tyr-211, Arg-397, Ala-303	Asp-382, Gly-302, Gly-210, Thr-304, Gly-279
4	-6.5	Ala-303	Gly-279, Gly-302, Ala-278, Phe-209, Tyr-211	Val-309, Gly-210, Thr-304
Amoxicillin	-7.3	Glu-305, Asp-299, Thr-323, Gly-279, Gly-302	Ile-301, Pro-281, Ser-280, Asp-382	Tyr-378, Thr-380, Arg-378, Gly-300, Leu-282

3.6. *In-silico* prediction of drug-likeness, and pharmacokinetic prediction

Drug-likeness is a prediction that determines whether a specific organic molecule has qualities that indicate it could be an orally active drug (Lipinski, *et al*. 2001). The isolated compounds' drug-likeness was assessed using "Lipinski's rule of five," which specifies that prospective molecules should have (MW≤500, ilog P≤5, H-bond donors ≤5, and H-bond acceptors ≤10) (Lipinski *et al*., 2001) and Veber's parameters (TPSA ≤140 $Å^2$ and rotatable bonds≤10) (Veber *et al*., 2002). Compounds **1, 3**, and **4** fulfill Lipinski's rule of five, indicating that they are drug-like and potentially orally active (Table 12). Furthermore, all the isolated compounds showed relatively better bioavailability scores of 0.55, indicating drug-like characteristics (Martin 2005). Their Hemoglobin D disease (HBD) values are <3, indicating greater solubility in cellular membranes, and their hemoglobin A (HBA) values range from 1 to 5. The ilog P values for all compounds are <5, with compounds **3** and **4** having particularly good lipophilic characteristics, indicating a favorable balance between solubility and permeability. The TPSA values of the compounds ranged from 20.23 to 66.76, which is < 140$Å^2$, indicating that intestinal absorption is good and that the drug does not have passive cellular permeability if the limits are higher than the score (Turner *et al*., 2004). Using the formula % Abs= 109 - 0.345 TPSA (Remko 2009), the percentage absorption analysis of the compounds (Table 12) revealed that all of the isolated compounds had higher percent absorption than the control. Their molar refractive index values,

which range from 34.59 to 123.14, indicate the likelihood that they could be developed to drugs.

The ability of molecules to penetrate the outer layer of the skin is described by skin permeability (Kp). The isolated compounds' log Kp values (Table 13) were all determined to be within the permissible range of -2.77 to -6.71. The SwissADME prediction parameters have shown that the GIA exhibits good oral absorption except for compound **2**. The results of the BBB permeability test performed on tested compounds (Table 13) demonstrated that compounds **2** and **4** lack BBB permeability.

In this study, compound **1** inhibited all cytochrome P_{450}s except for CYP2D6 and CYP3A4, while the others showed no inhibitory properties except for compounds **2** and **3**, which inhibited CYP2C9 and CYP3A4, respectively (Table 13). Furthermore, glycoprotein inhibition measurements were used to predict target compound excretion properties. P-gp and cytochrome P_{450} are known to help protect biofilms (gastrointestinal tract or brain) from exogenous substance efflux (biotransformation) to protect tissues (Finch and Pillans 2014). All of the compounds (**1-4**) exhibited no inhibition of P-gp, so no liver dysfunction effects are expected after administration.

The pharmacokinetics were also evaluated using the boiled egg model, which allowed for the prediction of gastrointestinal (GI) absorption and blood-brain barrier (BBB) penetration with the alignment of lipophilicity (WlogP) and polarity (TPSA) properties. The white region indicated a high likelihood of passive absorption by the gastrointestinal tract, while the yellow region (yolk) indicated a high likelihood of brain penetration. Yolk and white areas did not have to be mutually exclusive. Furthermore, the points were colored blue if it was predicted to be actively effluxed by P-gp (PGP+) and red if it was predicted to be a non-substrate of P-gp (PGP-).

The boiled-egg (Figure 3) prediction model showed that compound **4** was predicted as passively absorbed but not accessing the brain (in the white) and PGP– (red dot), whereas, compound **1** and **3** was predicted as brain-penetrant (in the yolk) and not subjected to active efflux (red dot). Compound **2** and the standard drug amoxicillin were predicted as not absorbed and not brain penetrant (outside the Egg).

All compounds were found to be inactive in all toxicological endpoints except for compounds **1** and **2** that were predicted to be immunotoxin. From the results shown in Table 14, it is possible to deduce that the compounds can have acceptable profile as a lead for the development of safe and effective drugs in the future. The predicted LD_{50} (mg/kg) for the tested compounds range from 650 to 3800, and their toxicity class as classified by Pro Tox-II ranges from grade 3 to 5.

Table 12: Calculated parameters of *in silico* bioavailability (drug-likeness) prediction & physicochemical properties of the isolated compounds (**1-4**) and amoxicillin

Compound	MW (g/mol)	NRB	NHBA	NHBD	MR	TPSA	%Abs	iLog P	Log S (ESOL)	Lipinski violations	Synthetic accessibility	Bioavailability score
1	292.37	10	4	1	84.79	55.76	89.76	3.9	-4.66	0	2.89	0.55
2	384.64	4	1	1	123.14	20.23	102.02	4.73	-7.17	1	5.9	0.55
3	124.14	1	2	2	34.59	40.46	95.04	1.31	-1.35	0	1	0.55
4	184.15	2	4	2	41.92	66.76	115.97	1.2	-2.29	0	1.4	0.85
Amoxicillin	365.40	5	6	4	94.56	158.26	54.40	3.17	-0.7	0	6.51	4.17

Table 13: Pharmacokinetic (ADME) properties prediction of the isolated compounds **1-4**

Compounds	GI abn	BBB per	Pgp sub	CYP1A2 Inhibitor	CYP2C19 Inhibitor	CYP2C9 Inhibitor	CYP2D6 Inhibitor	CYP3A4 Inhibitor	log Kp (cm/s)
1	High	Yes	No	Yes	Yes	Yes	No	No	-4.19
2	Low	No	No	No	No	Yes	No	No	-2.77
3	High	Yes	No	No	No	No	No	Yes	-6.71
4	High	No	No	No	No	No	No	No	-6.01
Amoxicillin	Low	No	No	No	No	No	No	No	-9.94

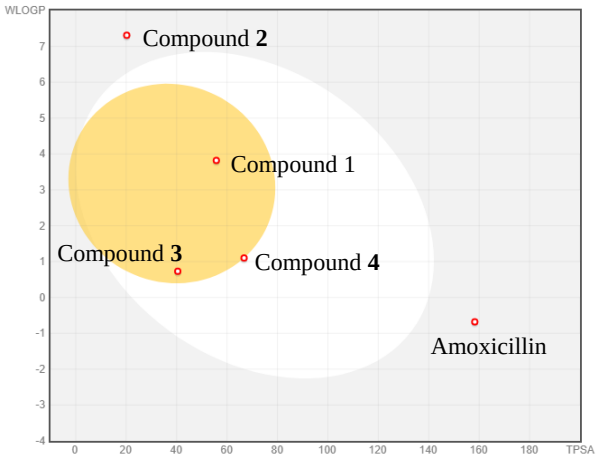

Figure 3: BOILED-Egg model for predicting gastrointestinal absorption and brain access

Table 14: *In silico* pharmacodynamics (toxicity) prediction of compounds **1-5** and amoxicillin using Pro Tox-II online servers

Compounds	Hepato-toxicity	Carcino-genicity	Immuno-toxicity	Mutagen-icity	Cyto-toxicity	LD_{50} (mg/Kg)	Toxicity Class
1	Inactive	Inactive	Active	Inactive	Inactive	3800	5
2	Inactive	Inactive	Active	Inactive	Inactive	890	4
3	Inactive	Inactive	Inactive	Inactive	Inactive	650	3
4	Inactive	Inactive	Inactive	Inactive	Inactive	1800	4
Amoxicillin	Inactive	Active	Inactive	Inactive	Inactive	2991	4

4. Conclusions

Gloriosa superba has been traditionally attributed to a wide range of therapeutic actions and ethno-medicinal uses. Natural products represent an important source of new lead compounds in drug discovery research. The present study identified the presence of caffeic acid derivative (**1**), desmosterol (**2**), two phenolic derivatives (**3**, **4**) and two disaccharides (**5**, **6**) in the study plant. Compounds **1-4** are reported herein for the first time from the species. The *in vitro* antibacterial and radical scavenging activity, and the molecular docking analysis suggest the potential use of the extracts of *G. superba* and compounds **1**, **2** and **4** as promising antibacterial agents and the extracts as promising free radical scavengers.

The compounds found here are from the chloroform and methanol crude. In later fractions, spots with promising yields were observed on TLC, but isolation proved challenging. This suggests that further studies, particularly employing advanced chromatographic

techniques, may be needed to isolate additional compounds. Further biological activity, such as antifungal, anticancer, and cytotoxicity, on crude extracts are required to validate the traditional use of the plant. Additionally, 2D NMR spectroscopic techniques (HMBC, HSQC, COSY, and NOESY) and MS studies are required to have a better understanding of structural and chemical parameters required to develop related drug lead compounds.

Acknowledgements: The authors acknowledge Adama Science and Technology University for funding part of the work. The support rendered by the Adama Public Health Research & Referral Lab Center of Adama, Ethiopia, during the antibacterial study is also gratefully acknowledged.

Reference

Ayele, T. T. (2018). A Review on Traditionally Used Medicinal Plants/Herbs for Cancer Therapy in Ethiopia: Current Status, Challenge and Future Perspectives. *Org. Chem. Curr. Res.*, 7(2), 192.

Babu, R. K., Rajanikanth, G., Rajesh, G., Mani, R. A., and Ramesh, N. (2018). Antimicrobial studies on seed extracts of Gloriosa superba L. *Int. J. Life Sci. Res., 6*(3), 499-508.

Belayneh, Anteneh., and Bussa, Negussie. (2014). Ethnomedicinal plants used to treat human ailments in the prehistoric place of Harla and Dengego valleys, eastern Ethiopia. *J. Ethnobiol. Ethnomed.*, 10(1), 18.

Brand-Williams, W., Cuvelier, M. E. and Berset, C. L. W. T. (1995). Use of a free radical method to evaluate antioxidant activity. *LWT - Food Sci Technol*, 28 (1), 25-30.

Chaudhary, S., El-Shorbagi, A. N., Shridhar, B., Gupta, M.K. and Verma, H. (2019). A Review on Phytochemical And Pharmacological Profile of *Gloriosa superba* Linn. *Int. Res. J. Pharm.*, 10(4), 1-5.

CLSI. (2018). Performance Standards for Antimicrobial Disk Susceptibility Tests, M02,. 13th ed, Clinical and Labratory Standards Institute, Wayne, PA.

Dar, R. A., Shahnawaz, M., Rasool, S. and Qazi, P. H. (2017). Natural product medicines: A literature update. *J. phytopharm.*, 6(6), 349-351.

Finch, A. and Pillans, P. (2014). P-glycoprotein and its role in drugdrug interactions. *Aust. Prescr.*, 37(4), 137-139.

Gopinath, K., Karthikeyan, C., Haja Hameed, A.S., Arunkumar, K. and Arumugam, A. (2015). Phytochemical Synthesis and Crystallization of Sucrose from the Extract of *Gloriosa superba*. *Res. J. Phytochem.*, 9, 144-160.

Hassan, A. K. M. S, and Roy, S. K., (2005). Micropropagation of Gloriosa superba L. through High Frequency Shoot Proliferation. *Plant Tissue Cult*, 15(1), 67-74

Itefa Degefa Alemu., and Tolessa Muleta Daba. (2016). Gloriosa, a source of colchicine:review article. *Int. J. Biol. Chem. Sci.*, 10 (4): 1888-1893.

Jagtap, S. and Rajendra, S. (2014). Phytochemical Screening, Antioxidant, Antimicrobial and Flavonoid Analysis of Gloriosa superba Linn. Rhizome Extracts. *J. Academia and Industrial Research*, 3(6), 247-254.

Jayakumar, F. A., Simon, S. E., Wei, Y. Y. and Woon, Y. P. (2018). Characteristic and optimized use of bioactive compounds from Gloriosa superba and Albizia amara with apoptotic effect on hepatic and squamous skin carcinoma. *Int J Pharm Sci Res*, 9(5), 1769-78.

Jonasson, E., Matuschek, E. and Kahlmeter, G., (2020). The EUCAST rapid disc diffusion method for antimicrobial susceptibility testing directly from positive blood culture bottles. *J. Antimicrob. Chemother.*, 75, 968-978.

Jothi, C., Anjelin, J., Gajalakshmi, D., and Sivakumar, T. (2019). Phytochemical Analysis and Evaluation of Antimicrobial Activity in the Whole Plant Extracts of *Gloriosa superba*. *Asian J Pharm Clin Res*, 12(6), 245-249.

Kumar, C. G., Mongolla, P., Pombala, S., Bandi, S., Babu, K. S. and Ramakrishna, K. V. (2017). Biological evaluation of 3-hydroxybenzyl alcohol, an extrolite produced by *Aspergillus nidulans* strain KZR-132. *J. Appl. Microbiol.*, 122(6), 1518-1528.

Legrand, S., Nordlander, G., Nordenhem, H., Borg-Karlson, A. K. and Unelius, C. R. (2004). Hydroxy- methoxybenzoic methyl esters: Synthesis and antifeedant activity on the pine weevil, *Hylobius abietis*. *Zeitschrift für Naturforschung. B, A J Chem Sci*, 59(7), 829-835.

Lipinski, C.A. (2016). Rule of five in 2015 and beyond: Target and ligand structural limitations, ligand chemistry structure and drug discovery project decisions. *Adv. Drug Deliv. Rev.*, 101, 34-41.

Lipinski, C.A., Lombardo, F., Dominy, B. W. and Feeney, P. J. (2001). Experimental and computational approaches to estimate solubility and permeability in drug discovery and development settings. *Adv. Drug Deliv. Rev.,* 46 (1-3), 3-26.

Martin, Y. C. (2005). A bioavailability score. *J. Med. Chem.,* 48 (9), 3164-3170.

Megala, S. and Elango, R. (2012). In Vitro Antibacterial Activity Studies of Tuber and Seed Extracts of *Gloriosa superba* Linn. *Int. J. Pharm. Sci. Res.,* 3(10), 4230-4234.

Nikhila, G. S., Sangeetha, G., Preetha, T. S. and Swapna, T. S. (2016). GC-MS analysis of phytochemical compounds present in the rhizome of *Gloriosa superba* L. *J. pharmacogn. phytochem.,* 5(5), 17-20.

Pallavi, S., and Tulika, M. (2022). *Gloriosa superba* L.: A Diminishing Wonder. *European J. Biomed. Pharm. Sci.s,* 9(12), 540-546.

Patil, P. B. and Gavade, R.T. (2012). *Gloriosa superba* Linn - A medicinally important plant. *Annals of Pharmacology and Pharmaceutical Science*, 3(2), 72-74.

Remko, M. (2009). Theoretical study of molecular structure, pKa, lipophilicity, solubility, absorption, and polar surface area of some hypoglycemic agents. *J. Mol. Struct.*, 897(1-3), 73-82.

Seeliger, D. and de Groot, B. L. (2010). Ligand docking and binding site analysis with PyMOL and Autodock/Vina. *J. Comput. Aided Mol. Des.*, 24, 417-422.

Simon, S. E. and Jayakumar, F.A. (2016). Antioxidant Activity and Anticancer Study on Phytochemicals Extract from Tubers of *Gloriosa superba* against Human Cancer Cell (Hep-G2). *J. pharmacogn. phytochem.*, 4(4), 7-12.

Solomon Tesfaye, Kaleab Asres, Ermias Lulekal, Yonatan Alebachew, Eyael Tewelde, Mallika Kumarihamy3, Ilias Muhammad. (2020). Ethiopian Medicinal Plants Traditionally Used for the Treatment of Cancer, Part 2: A Review on Cytotoxic, Antiproliferative, and Antitumor Phytochemicals, and Future Perspective. *Molecules*, 25(17), 4032.

Takenaka, M., Yan X., Ono H., Yoshida M., Nagata T. and Nakanishi T. (2003). Caffeic Acid Derivatives in the Roots of Yacon (*Smallanthus sonchifolius*). *J. Agric. Food Chem.,* 51(3), 793-796.

Teklehaymanot, Tilahun. (2009). Ethnobotanical study of knowledge and medicinal plants use by the people in Dek Island in Ethiopia. *J. Ethnopharmacol.*, 124(1), 69-78.

Trott, O. and Olson, A. J. (2010). AutoDock Vina: improving the speed and accuracy of docking with a new scoring function, efficient optimization, and multithreading. *J. Comput. Chem.*, 31, 455-461.

Tulika, M. and Pallavi, S. (2020). A Critical Review of Glory Lily: A Rare Medicinal Plant. *World J Pharm Pharm Sci*, 9(10), 1123-1133.

Turner, J. V., Maddalena, D. J., Agatonovic-Kustrin, S. (2004). Bioavailability prediction based on molecular structure for a diverse series of drugs. *Pharm. Res.*, 21(1), 68-82.

Umavathi, S., Gopinath, K., Manjula, M. S., Balalakshmi, C. and Arumugam, A. (2020). *Gloriosa superba* L: A critical Review of Recent Advances. *Abasyn J Life Sci.*, 3 (2), 48-65.

Veber, D. F., Johnson, S. R., Cheng, H.-Y., Smith, B. R., Ward, K. W. and Kopple, K. D. (2002). Molecular properties that induence the oral bioavailability of drug candidates. *J. Med. Chem.*, 45(12), 2615-2623.

Warrier, P. K., Nambiar, V. P. K. and Ramankutty, C. (1995). *Indian Medicinal Plants.* Edited by Kottakkal Arya Vaidua Sala. Vol. 3. Orient Longman.

Wilson, W. K., Sumpter, R. M., Warren, J. J., Rogers, P. S., Ruan, B. and Schroepfer, G. J. (1996). Analysis of unsaturated C_{27} sterols by nuclear magnetic resonance spectroscopy. *J Lipid Res.*, 37, 1529-1555.